J|A|C|S
ARTICLES
Published on Web 12/12/2003

Mechanism of Homogeneous Ir(III) Catalyzed Regioselective Arylation of Olefins

Jonas Oxgaard,[†] Richard P. Muller,[†] William A. Goddard, III,*[,†] and Roy A. Periana[‡]

Contribution from the Materials and Process Simulation Center, Beckman Institute (139−74), Division of Chemistry and Chemical Engineering, California Institute of Technology, Pasadena, California 91125, and University of Southern California, Department of Chemistry, Loker Hydrocarbon Institute, Los Angeles, California 90089

Received January 11, 2003; E-mail: wag@wag.caltech.edu

Abstract: The mechanism of hydroarylation of olefins by a homogeneous Ph-Ir(acac)$_2$(L) catalyst is elucidated by first principles quantum mechanical methods (DFT), with particular emphasis on activation of the catalyst, catalytic cycle, and interpretation of experimental observations. On the basis of this mechanism, we suggest new catalysts expected to have improved activity. Initiation of the catalyst from the inert trans-form into the active cis-form occurs through a dissociative pathway with a calculated ΔH(0 K)$^{\ddagger} = 35.1$ kcal/mol and ΔG(298 K)$^{\ddagger} = 26.1$ kcal/mol. The catalytic cycle features two key steps, 1,2-olefin insertion and C−H activation via a novel mechanism, oxidative hydrogen migration. The olefin insertion is found to be rate determining, with a calculated ΔH(0 K)$^{\ddagger} = 27.0$ kcal/mol and ΔG(298 K)$^{\ddagger} = 29.3$ kcal/mol. The activation energy increases with increased electron density on the coordinating olefin, as well as increased electron-donating character in the ligand system. The regioselectivity is shown to depend on the electronic and steric characteristics of the olefin, with steric bulk and electron withdrawing character favoring linear product formation. Activation of the C−H bond occurs in a concerted fashion through a novel transition structure best described as an oxidative hydrogen migration. The character of the transition structure is seven coordinate Ir^{V}, with a full bond formed between the migrating hydrogen and iridium. Several experimental observations are investigated and explained: (a) The nature of L influences the rate of the reaction through a ground-state effect. (b) The lack of β-hydride products is due to kinetic factors, although β-hydride elimination is calculated to be facile, all further reactions are kinetically inaccessible. (c) Inhibition by excess olefin is caused by competitive binding of olefin and aryl starting materials during the catalytic cycle in a statistical fashion. On the basis of this insertion-oxidative hydrogen transfer mechanism we suggest that electron-withdrawing substituents on the acac ligands, such as trifluoromethyl groups, are good modifications for catalysts with higher activity.

1. Introduction

The synthesis of straight-chain alkyl benzenes is generally complicated by the almost 100% selectivity toward the branched isomer in conventional Friedel−Crafts alkylation. Even though the use of shape selective zeolites has met some limited success,[1] the method of choice is normally a Friedel−Crafts acylation followed by reduction. Recently, Matsumoto[2−4] and Periana[5] reported the synthesis of a novel Ir complex, [Ir(μ-acac-O,O,C^3)-(acac-O,O)(acac-C^3)]$_2$, **4**, that catalyses arylation of an unactivated olefin by benzene, generating a mixture of linear and branched alkyl benzenes (see Figure 1). Although potentially a very useful catalyst, several unresolved issues impede commercialization. Foremost among these are the low activity (turnover-frequency (TOF) of 10^{-3} s^{-1} at 200 °C), but there are also problems with selectivity, cost, and stability.

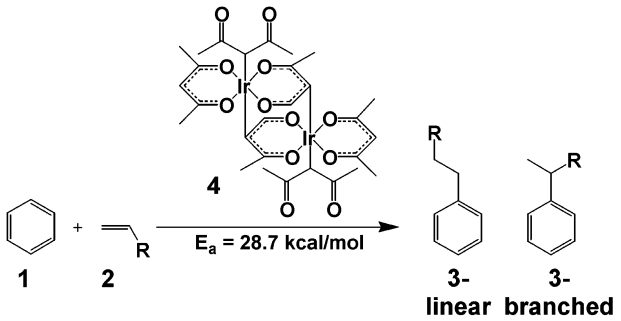

Figure 1. Arylation of olefin catalyzed by **4**.

Here, we explore the mechanism of hydroarylation of olefins by a Ph-Ir(acac)$_2$(L) catalyst on the ΔH(0 K) and ΔG(298 K) surfaces. In particular, the following questions will be addressed:

(i) How is the catalytic cycle initiated?

[†] Materials and Process Simulation Center, Beckman Institute (139−74), Division of Chemistry and Chemical Engineering, California Institute of Technology.

[‡] University of Southern California, Department of Chemistry, Loker Hydrocarbon Institute.

(1) Fraenkel, D.; Levy, M. *J. Catal.* **1989**, *118*, 10. (b) Cao, Y.; Kessas, R.; Naccache, C.; Taarit, Y. B. *Appl. Catal. A* **1999**, *184*, 231.
(2) Matsumoto, T.; Taube, D. J.; Periana, R. A.; Taube, H.; Yoshida, H. *J. Am. Chem. Soc.* **2000**, *122*, 7414.
(3) Matsumoto, T.; Periana, R. A.; Taube, D. J.; Yoshida, H. *J. Mol. Catal. A* **2002**, 1.
(4) Matsumoto, T.; Yoshida, H. *Catal. Lett.* **2001**, *72*, 107.
(5) Periana, R. A.; Liu, Y. X.; Bhalla, G. *Chem. Commun.* **2002**, 3000.

10.1021/ja034126i CCC: $27.50

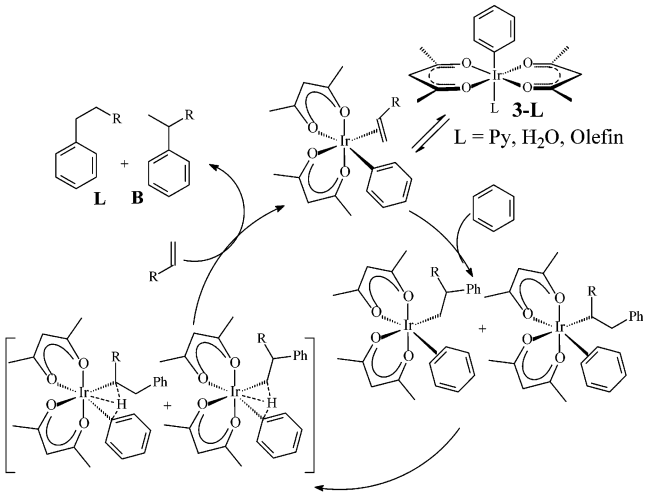

Figure 2. Catalytic cycle proposed by Periana.

(ii) What is the mechanism of the catalytic cycle?

(iii) What is the rate-determining step?

(iv) What is the origin of the regioselectivity for olefin insertion?

(v) By what mechanism is the C−H bond activated?

(vi) Why is no β-hydride elimination observed to form unsaturated products?

(vii) Why is the reaction inhibited by excess olefin?

(viii) How can the activity and selectivity of the catalyst be improved?

Matsumoto[3] and Periana[5] have conducted mechanistic studies, showing that C−H activation is involved and excluding several potential mechanisms. However, an unambiguous mechanism for the C−H activation and other critical steps has not yet been determined. Matsumoto concluded that the mechanism is not related to the Friedel−Crafts mechanism, and measured the free energy of activation for the unsubstituted reaction to be 28.7 kcal/mol. Both selectivity and activity change when substituted olefins are used, whereas activity changes with substituted aryls. The reaction exhibits complex kinetic behavior with nonzero order in ethene at low ethene/benzene ratios, but a negative dependence at higher ratios, indicating competitive inhibition by ethene. Periana showed, Figure 2, that the active catalyst is most likely a mononuclear Ph-Ir(acac)$_2$ or Ph-Ir(acac)$_2$(L) compound formed from arene C−H activation, where L is a coordinating ligand such as H_2O or pyridine. This hypothesis was strengthened by the independent synthesis of several mononuclear Ph-Ir(acac)$_2$(L) compounds, Figure 3, all of which have catalytic activities similar to **4**. Furthermore, the mechanism does not appear to contain any charged species or breaking of Ir−O bonds between Ir and the acac ligands, which significantly reduces the number of potential mechanistic pathways.

The mechanism suggested by Periana[5] features activation of the starting catalysts, which includes isomerization of the trans-Ph-Ir(acac)$_2$(L) to a cis-Ph-Ir(acac)$_2$(L) compound and coordination of the olefin. 1,2-Migration of the phenyl group to ethene, as observed in the Heck reaction, and coordination of a second benzene leads to a covalently bound Ir-alkyl species. C−H activation and hydrogen migration yields alkyl benzene and an Ir-phenyl compound. The C−H activation was expected to proceed either through a seven-coordinate Ir^{V} intermediate or through a σ-bond metathesis pathway, as suggested for analogous C−H activations by the groups of Bergman[6] and Maitlis.[7] Replacement of the alkyl benzene with an olefin completes the catalytic cycle. The identity of the rate determining step or the basis for the varying activies and selectivities observed with different olefinic substrates and additives have not yet been experimentally determined.

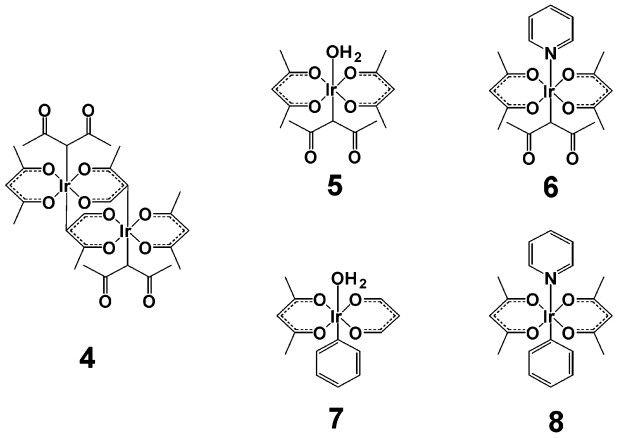

Figure 3. Starting catalysts **4**−**8**.

2. Computational Methodology

All calculations were performed using the hybrid DFT functional B3LYP as implemented by the Jaguar 4.1 program package.[8] This DFT functional utilizes the Becke three-parameter functional[9] (B3) combined with the correlation functional of Lee, Yang, and Par[10] (LYP) and is known to produce good descriptions of reaction profiles for transition metal containing compounds.[11,12] The Ir was described by the Wadt and Hay[13] core-valence (relativistic) effective core potential (treating the 17 electrons explicitly) using the LACVP basis set with the valence double-ζ contraction of the basis functions, LACVP**. All electrons were used for all other elements using a modified variant of Pople's[14] 6-31G** basis set, where the six d functions have been reduced to five.

Implicit solvent effects of the experimental benzene medium were calculated with the Poisson−Boltzmann (PBF) continuum approximation,[15] using the parameters $\epsilon = 2.284$ and $r_{solv} = 2.602$ Å. Due to the increased cost of optimizing systems in the solvated phase (increase in computation time by a factor of ~4) solvation effects are calculated here as single point solvation corrections to gas-phase geometries. Control calculations on structures **7** and **TS2** show that energies change only 0.12 and 0.33 kcal/mol, respectively, when optimized in solution.

(6) Tellers, D. M.; Yung, C. M.; Arndtsen, B. A.; Adamson, D. R.; Bergman, R. G. *J. Am. Chem. Soc.* **2002**, *124*, 1400. (b) Klei, S. R.; Tilley, T. D.; Bergman, R. G. *J. Am. Chem. Soc.* **2000**, *122*, 1816. c) Alaimo, P. J.; Bergman, R. G. *Organometallics* **1999**, *18*, 2707.
(7) Isobe, K.; Miguel, A. V. d.; Nutton, A,; Maitlis, P. M. *J. Chem. Soc., Dalton Trans.* **1984**, 929. (b) Isobe, K.; Bailey, P. M.; Maitlis, P. M. *J. Chem. Soc., Chem. Commun.* **1981**, 808.
(8) Jaguar 4.1, Schrodinger, Inc., Portland, Oregon, 2000.
(9) Becke, A. D. *J. Chem. Phys.* **199**3, *98*, 5648.
(10) Lee, C.; Yang, W.; Parr, R. G. *Phys. Rev. B* **1988**, *37*, 785.
(11) Baker, J.; Muir, M.; Andzelm, J.; Scheiner, A. In *Chemical Applications of Density-Functional Theory*; Laird, B. B., Ross, R. B., Ziegler, T., Eds.; ACS Symposium Series 629; American Chemical Society: Washington, DC, 1996.
(12) Niu, S.; Hall, B. M. *Chem. Rev.* **2000**, *100*, 353.
(13) Hay, P. J.; Wadt, W. R. *J. Chem. Phys.* **1985**, *82*, 299. (b) Goddard, W. A., III *Phys. Rev.* **1968**, *174*, 659. (c) Melius, C. F.; Olafson, B. O.; Goddard, W. A., III *Chem. Phys. Lett.* **1974**, *28*, 457.
(14) Hariharan, P. C.; Pople, J. A. *Chem. Phys. Lett.* **1972**, *16*, 217. (b) Francl, M. M.; Pietro, W. J.; Hehre, W. J.; Binkley, J. S.; Gordon, M. S.; DeFrees, D. J.; Pople, J. A. *J. Chem. Phys.* **1982**, *77*, 3654.
(15) Tannor, D. J.; Marten, B.; Murphy, R.; Friesner, R. A.; Sitkoff, D.; Nicholls, A.; Ringnalda, M.; Goddard, W. A., III.; Honig, B. *J. Am. Chem. Soc.* **1994**, *116*, 11 875. (b) Marten, B.; Kim, K.; Cortis, C.; Friesner, R. A.; Murphy, R. B.; Ringnalda, M. N.; Sitkoff, D.; Honig, B. *J. Phys. Chem.* **1996**, *100*, 11 775.

Geometries, frequencies, and zero point energies were also largely unchanged (see the Supporting Information for structures with and without solvation). Furthermore, control calculations of **TS2**(2,2)-propene and **TS2**(1,2)-propene in solution changed $\Delta\Delta H$(0 K) less than 0.1 kcal/mol.

Energies on the ΔH(0 K) surface are reported as ΔE + zero point energy corrections at 0 K + solvation correction. Energies on the ΔG(298 K) surface are reported as ΔE + zero point energy corrections at 0 K + solvation correction + ΔG corrections at 298 K.

Relative energies on the ΔH(0 K) surface are expected to be accurate to within 3 kcal/mol for stable intermediates, and within 5 kcal/mol for transition structures. Moreover, relative energies of iso-electronic species (such as regio-isomers) are considerably more accurate, since the errors largely cancel.

Relative energies on the ΔG(298 K) surface are significantly less accurate, due to the use of the PBF model.[16] Consequently, relative energies on the ΔG(298 K) surface can at best be considered qualitative, and should only be considered when comparing fairly similar species. This is further discussed in section 3.9.

All geometries were optimized and evaluated for the correct number of imaginary frequencies through vibrational frequency calculations using the analytic Hessian. Zero imaginary frequencies correspond to a local minimum, whereas one imaginary frequency corresponds to a transition structure. Due to a documented bug in the Jaguar implementation of frequency calculations on Ir,[17] all imaginary frequencies between 0 and -30 cm^{-1} were ignored. This bug has subsequently been corrected in Jaguar 5.0. Although the singlet states are expected to be the lowest energy spin states, we also investigated higher spin states for select geometries, and invariably found the singlet as the lowest energy state.

To reduce computational time the methyl groups on the acac ligands were replaced with hydrogens. Control calculations show that relative energies of intermediates and transition structures change less than 0.1 kcal/mol when methyl groups are included. Regioselectivites are also largely unaffected. The use of a truncated acac group is here labeled acac†.

3. Results and Discussion

3.1 Preliminaries. 3.1.1 Net Reaction. The reaction of benzene (**1**) and ethene (**2**) to generate ethyl benzene (**3**), illustrated in eq 1, is calculated to be exothermic with ΔH(0 K) = -21.7 kcal/mol and ΔH(289.15 K) = -23.9 kcal/mol, which corresponds very well to the experimental value of ΔH(289.15 K) = -25.2 kcal/mol.[18] We calculate ΔG(289.15 K) = -15.4 kcal/mol, very close to the experimental value of -16.1 kcal/mol.[18] Adding single point solvation correction to the gas-phase geometries reduces the exothermicity by 0.9 kcal/mol. This small correction reflects the similar hydrophobicity of starting materials and reactants. No experimental value could be found for the reaction in benzene.

$$C_2H_4 + C_6H_6 \rightarrow \text{ethyl benzene } \Delta H(289.15\text{ K}) = -23.9\text{ kcal/mol} \quad (1)$$

3.1.2 Character of the Bonding. Species such as **5**−**8** are generally described as Ir^{III}, which assumes that the acac ligands each get one electron from the metal while the phenyl or C-bonded acac group gets another for a total of three oxidations of the Ir. This is an oversimplification, because the Ir−C bonds are quite covalent. QM calculations show that the two electron

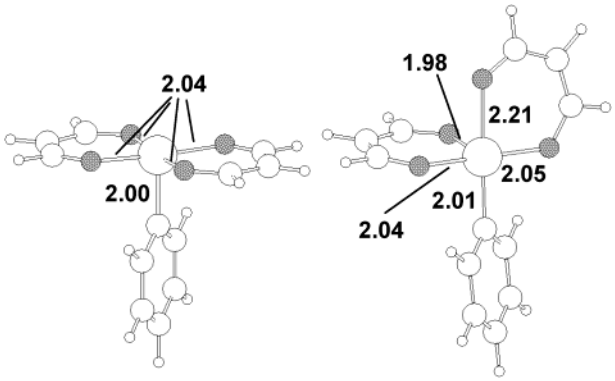

Figure 4. Structures **10** and **11**. Bond lengths in Angstroms (Å).

Ir−C sigma bond has about one electron in an Ir orbital with dominantly dz^2 character and the other in a sp^2 orbital on the carbon. This single bond has a length of 2.11, 2.16, 2.01, and 2.03Å in **5**−**8**, respectively. The bonding to each acac can be thought of as a resonance of two configurations each with a covalent bond, say in the *x* direction, and a donor−acceptor in the *y* direction. This leads to an average bond distance of 2.04, 2.05, 2.04, and 2.05 Å for **5**−**8**, which can be thought of as an average of a single bond of ∼1.90 Å and a D−A bond of ∼2.20 Å. This uses a combination of 6s and 5dx^2-y^2 character. The Ir has, in addition to the three electrons involved in the covalent bonds, 2 electrons each in the d*xy*, d*xz*, and d*yz* orbitals for a total of 9 electrons. In this Generalized Valence Bond (GVB) model the notation Ir^{III} refers to the three covalent bonds.

The ligand trans to the Ir−C localized covalent bond cannot make a partially covalent bond, thus in the cis compound **11** discussed below, the acac† O trans to the Ir−C bond becomes pure DA, with a bond distance of 2.21 Å, whereas the other bond to this acac† decreases to 2.04 Å. Thus, this acac† favors just the one resonance configuration. Simultaneously the bonds to the second acac† (still in the *xy* plane) favor slightly the resonance configuration with the lone pair trans to the 2.04Å bond of the first acac†.

3.2 Ground-State Effects. In the results reported by Matsumoto[2−4] and Periana,[5] it was noted that starting with different catalyst compositions based on the Ir^{III}(acac)$_2$ fragment led to varying catalytic rates, but that the ratio of linear to branched alkyl arene addition product was independent of the catalyst composition. This strongly indicates that different catalyst compositions share a common rate determining step, and most likely share catalytic cycles.[19] In this scenario, the change in catalyst rates with different starting catalysts is assumed to be caused by a ground state effect. This assumption was confirmed through theoretical calculations on the catalysts illustrated in Figure 3, which were experimentally investigated by Periana.[5] To compare the starting catalysts we report their relative energies. These relative energies can be considered

(16) Truong, T. N.; Truong, T. T.; Stefanovich, E. V. *J. Chem. Phys.* **1997**, *107*, 1881. (b) Cramer, C. J.; Thrular, D. G. *Chem. Rev.*, **1999**, *99*, 2161.
(17) Cao, Y.; Schrodinger, Inc., Portland, Oregon, Personal communication
(18) Design Institute for Physical Property Data (DIPPR) Project 801, http://dippr.byu.edu/.

(19) During review, one of the referees pointed out that the distribution of *n*-propyl benzene vs i-propyl benzene corresponds to the thermodynamic equilibrium distribution. However, this appears to be coincidental. Preliminary experimental studies show that i-propyl benzene is not susceptible to isomerization, either to *n*-propyl benzene or other products, when heated to 200 °C with the catalyst, **7**, in liquid benzene (with or without ethylene). This shows that the reaction cannot be under thermodynamic control. Preliminary calculations also show that the product distribution from higher alkenes do not correspond to the thermodynamic distribution. For example, the equilibrium distribution of 2-methyl-propyl benzene vs *tert*-butyl benzene is calculated to 97: 3, whereas the distribution observed in ref 3 is reported as 82:18.

Table 1. Activity and Relative Energy of Catalysts **4**−**8**

	experimental[a] (180 °C)		theoretical	
complex	TOF ($\times 10^{-4}$ s^{-1})	isomer ratio[b]	ΔH(0 K) (kcal/mol)	ΔG(298 K) (kcal/mol)
4	110	61:39	3.3	9.5
5	100	61:39	−1.0	4.6
6	24	61:39	−9.9	−2.4
7	130	61:39	0.0	0.0
8	32	61:39	−7.0	−5.0

[a] From ref 5. [b] Linear:branched product.

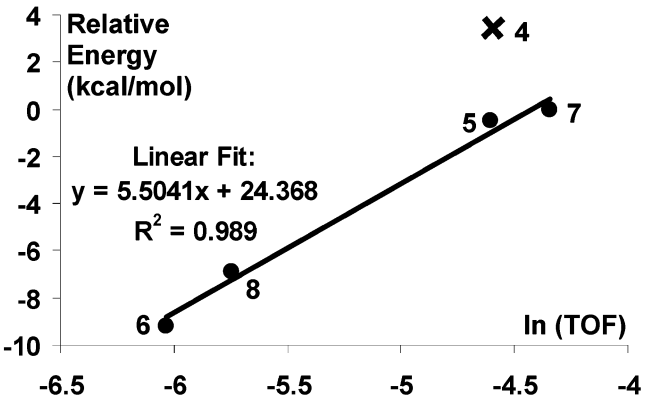

Figure 5. Plot of ln(TOF) vs ΔH of catalysts **4**−**8**. Line fitted to **5**−**8** with $R^2 = 0.989$. **4** not included due to chelating effects.

implicit reaction energies: the relative energy of, for example, **7** vs **5** is thus defined as the reaction energy of **7** + $C_5H_5N \rightarrow$ **5** + H_2O. The results of these calculations are summarized in Table 1, with the relative energy of **7** arbitrarily set to 0.

The activation energy of a catalyst is linearly related to the natural logarithm of the turnover frequency (TOF) by the Arrhenius equation, $k = Ae^{(-\Delta E/RT)}$. If the catalysts share the same rate determining step, then the activation energy, $\Delta E^{\ddagger}_{x,}$ for each catalyst x should be given by the expression $\Delta E^{\ddagger}_{x} = E_{rds} - E_x$, where E_x is the relative energy of the catalyst x, and E_{rds} is the relative energy of the rate determining step. If E_{rds} is the same for all the catalysts, then E_{rds} will be constant and we should thus expect to obtain a linear correlation between the natural logarithm of the experimentally derived TOFs and the calculated relative energies.

As can be seen in Figure 5, such a linear correlation for the monomeric catalysts **5**−**8** is clearly observed. The dimeric catalyst **4** is slightly off, which we believe is caused by chelating effects in the dimeric catalyst. *This confirms our hypothesis of a common rate-limiting step regardless of starting catalyst.* On the basis of these results and the similarities in product ratios, it is reasonable that catalysts **4**−**8** proceed through a similar reaction mechanism, illustrated in Figure 6, involving activation and cis−trans isomerization to the active catalyst **9**. As the above catalysts feature common mechanisms, we elected to limit this study to the most active catalyst, **7**.

3.3 Catalyst Activation by Cis−Trans Isomerization of Catalyst Precursor. There are several plausible mechanisms for the activation and conversion of **7** to **9**, the energetics of which are summarized in Figure 7. They all start with a barrierless dissociation of the H_2O ligand to yield the 5-coordinate, 16e$^-$ species **10**, 11.9 kcal/mol higher in energy than **7**. From **10**, one can continue on the dissociative pathway by rearrangement of the trans species **10** to the iso-electronic cis

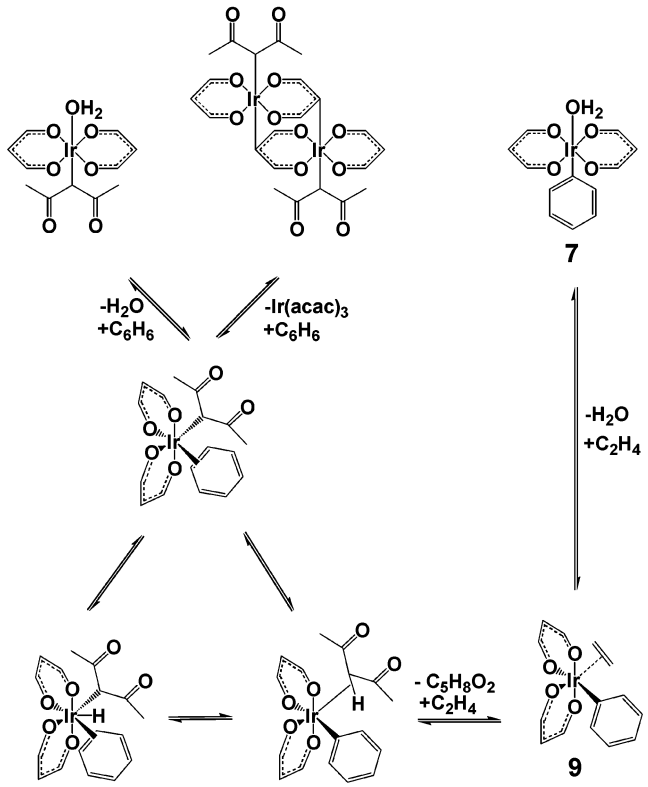

Figure 6. Suggested pathways for initiation of **4**−**8**.

species, **11**. Species **11** is 19.6 kcal/mol higher than the iso-electronic **10**. This is due to the loss of resonance stabilization in **1** as described in section 3.1.2. The transition structure **TS1A** (see Figure 8) connecting **10** and **11** has an activation energy of 23.2 kcal/mol relative to **10**, (35.1 kcal/mol relative to the resting state **7**) and a negative mode of −93 cm^{-1}, corresponding to a movement of the O−Ir−O angle. As **11** is significantly uphill in energy, it is not surprising that **TS1A** is a late transition structure with an O−Ir−O angle of 115.5° and an Ir−O bond length of 2.18 Å.

Species **10** can also continue via an associative pathway where it coordinates an ethene to give **12**, which is exothermic by 6.8 kcal/mol. From **12**, we explored the possibility of a concerted mechanism in which one of the Ir−O bonds would switch place with the Ir−(C_2H_4) group. However, we could not find a transition state connecting **12** and **9**. Forcing the O−Ir−O angle to go continuously from 180° to 90° invariably caused breaking of one of the Ir−O bonds. Likewise, forcing the (C_2H_4)−Ir−Ph angle from 180° to 90° led to dissociation of C_2H_4, regenerating **10**. Consistent with the experimental work showing lack of exchange of the acac ligands, deliberately breaking one of the Ir−O bonds gave structure **13**, 41.2 kcal/mol uphill from **12**. The magnitude of the barrier for this isomerization can be compared to the experimental values for racemization of the related $Ru(acac)_3$ and $Rh(acac)_3$, which are measured to be >40 kcal/mol.[20]

We also considered that coordination of C_2H_4 to **TS1A** might yield a transition structure **TS1B** (see Figure 8) that would bypass the high energy **11**. Simply adding a C_2H_4 to **TS1A** did not lead to a stable structure, however, so a more extensive mapping of the hypersurface was undertaken, and transition

(20) Fay, R. C.; Amal, Y. G.; Klabunde, U. *J. Am. Chem. Soc.* **1970**, *92*, 7056.

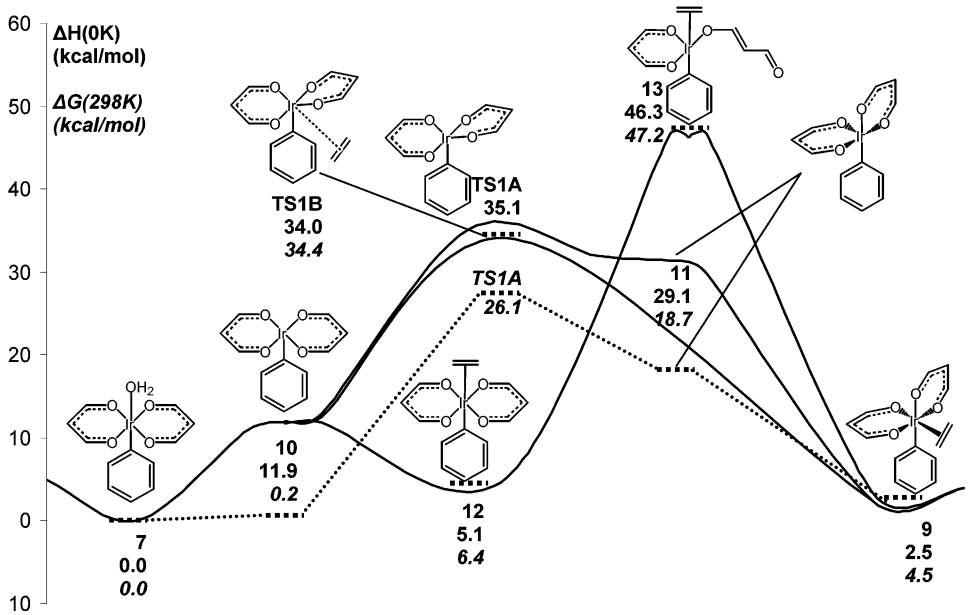

Figure 7. Pathways for converting the catalyst precursor **7** to the active catalyst **9**, deduced from QM calculations. The lowest energy pathway on the ΔG(298 K) surface is added in a simplified dotted line. The rate determining step is through **TS1A** with ΔH(0 K) = 35.1 kcal/mol and ΔG(298 K) = 26.1 kcal/mol. This is comparable to the experimental value of 28.7 kcal/mol at 413−473 K.

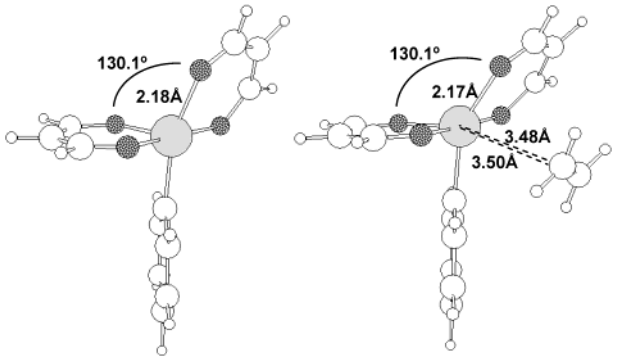

Figure 8. **TS1A** and **TS1B**.

structure **TS1B** was eventually located. **TS1B** has an activation energy of 22.1 kcal/mol relative to **10**, (34.0 kcal/mol relative to the resting state **7**), an O−Ir−O angle of 130.1° and a negative mode of −132 cm^{-1}, corresponding to movement of the O−Ir−O angle. The distances between the Ir and the carbons of the incoming C_2H_4 are calculated to 3.48 Å and 3.50 Å.

As **7** and **9** are quite close in energy, we also explored the possibility of adding C_2H_4 directly to **7**, which would lead to a transition structure **TS1C**. In this case, the incoming C_2H_4 could both stabilize the transition state and also induce the cis−trans isomerization. However, we could not locate **TS1C**, as all attempts of constraining the C_2H_4−Ir distance and the O−Ir−O angle resulted in breaking the Ir−O bond, at relative energies several kcal/mol higher than **TS1A** and **TS1B**.

Thus, the lowest energy pathways on the ΔH(0 K) surface are through **TS1A** or **TS1B**, with total activation energies of 35.1 and 34.0 kcal/mol. This is significantly higher than the experimental activation energy of 28.7 kcal/mol. However, including temperature and entropy corrections, we obtain ΔG values of 26.1 and 34.4 kcal/mol for **TS1A** and **TS1B**, respectively, indicating that **TS1A** is the preferred pathway. Although not quantitatively correct, it is clear that inclusion of entropy and temperature corrections are required to obtain an accurate picture of cis−trans isomerization. These estimates of entropy terms in liquid-phase assume the free translation and free rotation of dissociated products, which could cause errors of several kcal/mol. Nevertheless, the final energetics are in reasonable agreement with experiment, i.e., lower in energy than the experimental activation energy of 28.7 kcal/mol.

3.4 Catalytic Cycle. The important steps in the catalytic cycle derived from the QM calculations are given in Figure 9 (energy profile) and Figure 10 (structures), respectively.

3.4.1 Starting Point (9). The catalytic cycle starts with **9**, an Ir^{III} species featuring two acac† groups cis to each other, a covalently bound phenyl group and a coordinating C_2H_4 ligand. The C−*C* axis in the C_2H_4 ligand in **9** is parallel to the Ph−Ir−O axis, facilitating the migratory insertion found to be the first step in the catalytic cycle. The Ir−C1 and Ir−C2 distances are 2.25 Å, whereas the C1−C2 bond length is 1.40 Å. This indicates some small amount of iridium d → π^* back-bonding or of metallacyclepropane character.[21]

3.4.2 Migratory Insertion (9 → TS2 → 14). The migratory insertion proceeds via the transition structure **TS2**, with a relative energy of 27.0 kcal/mol. **TS2** is a four membered transition structure, featuring the simultaneous breaking of the Ir−C3(σ) and C1−C2(π) bonds and the creation of Ir−C1(σ) and C2−C3(σ) bonds. The geometric changes are as follows:

- The Ir−C3 distance increases from 2.05 Å in **9** to 2.20 Å at **TS2** to 2.41 Å in the product **14**.
- The C1−C2 distance increases from 1.40 Å in **9** to 1.47 Å in **TS2** to 1.54 Å in **14**.
- The Ir−C1 distance decreases from 2.25 Å in **9** to 2.08 Å in **TS2** to 2.0× Å in **14**
- The C2−C3 distance decreases from 2.25 Å in **9** to 1.90 Å in **TS2** to 1.52 Å in **14**.

Thus **TS2** has essentially fully formed Ir−C1 and C1−C2 single bonds, but half order bonds from C3 to Ir and to C2. **TS2** has one imaginary frequency of −348 cm^{-1}, corresponding

(21) Rappe, A. K.; Goddard, W. A. *J. Am. Chem. Soc.* **1982**, *104*, 297.

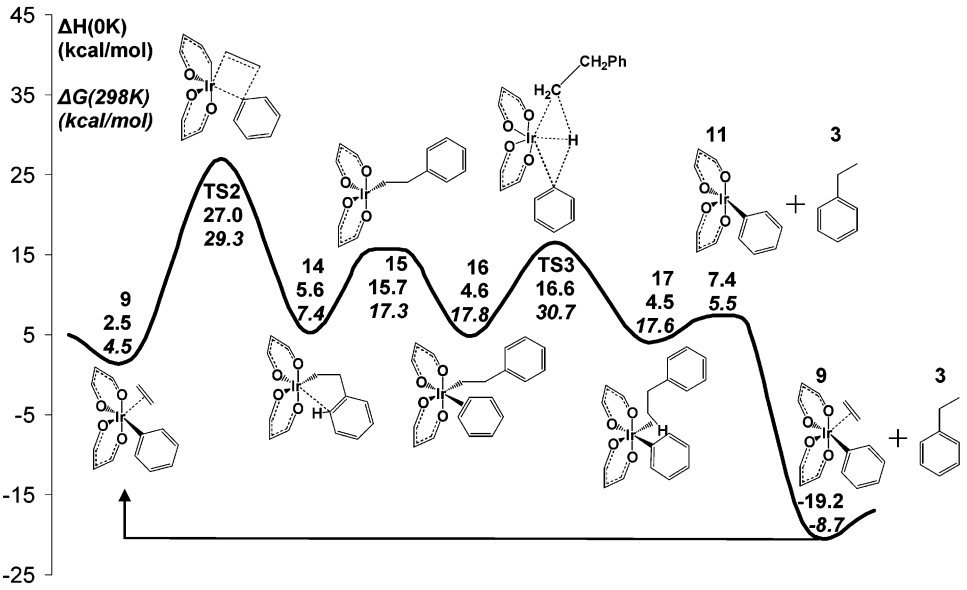

Figure 9. Calculated mechanism for generation of ethyl benzene.

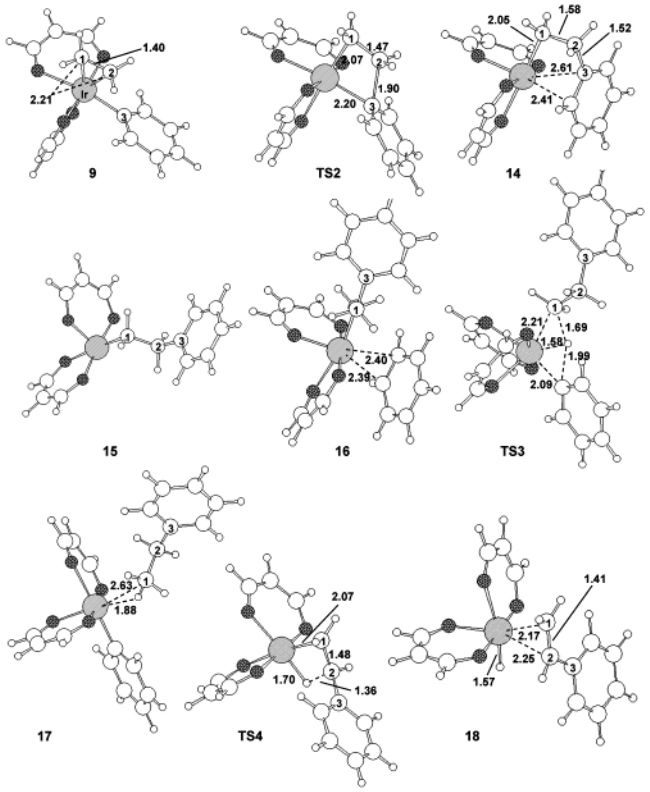

Figure 10. Structures of **9**, **14**−**18**, **TS2**−**TS4**. Distances in Angstroms (Å).

to a slipping of the C_2H_4 toward the phenyl group and closure of the C2−C3 distance.

The product of **TS2** is the intermediate **14** with a relative energy of 5.6 kcal/mol, 3.1 kcal/mol higher in energy than **9**. **14** features intramolecular coordination of the bound phenyl group, with Ir−C distances of 2.42 Å and 2.63 Å. The asymmetry in the coordination is caused by ring strain in the four membered ring formed by Ir−C1−C2−C3.

When compared with **15**, we consider that the coordination of the bound phenyl group is worth 10.1 kcal/mol, whereas comparing **9** with **11**, we can consider the coordination of the C_2H_4 group in **9** to be worth 29 kcal/mol (with Ir−C distances of 2.21 Å). Because the exothermicity to insert a free ethylene into the C−H bond of benzene [eq 1] is 23.9 kcal/mol, **14** has gained this amount by conversion of a π bond to a σ bond, but also lost 26.6−10.1 = 16.5 through the much weaker coordination of the phenyl vs the C_2H_4 group. Thus, if the Ir−C sp^2 bond in **9** were the same strength as the Ir−C sp^3 bond in **14**, we would have expected **14** to be 5.0 kcal/mol stable than **9**, rather than 3.1 kcal/mol less stable. This difference of 8.1 kcal/mol represents an increased strength of bonding in **9** due to the Ir−C sp^2 bond and π interactions with the phenyl group.

3.4.3 Addition of Benzene (14 → 15 → 16). The weak coordination of the phenyl group in **14** enables the next step in the cycle to be energetically accessible. Rotation around the C2−C3 bond leads to dissociation of the coordinating phenyl to form intermediate **15**. The energy cost is 10.1 kcal/mol uphill (with no additional barrier).

Association of a benzene to **15** to form **16** is exothermic by 11.1 kcal/mol, which can be compared to the 26.6 kcal/mol bond of ethylene to **11**. This is consistent with the Ir−C bonds of 2.39 and 2.40 Å for benzene in **16**, compared with the 2.21 Å Ir−C distances in **9**. The lack of steric strain in **16** makes it 1.0 kcal/mol more stable than **14**. The steric strain is most likely worth more than 1.0 kcal/mol, but the coordinated benzene moiety in **14** also features a small substituent effect from the electron donating $-CH_2-$ group, which increases the stabilization. A better measure of the coordination might be found by comparing the relative energy of the analogue of **15** with a coordinating toluene instead of benzene.

3.4.4 Hydride Transfer (16 → TS3 → 17). The final step in the functionalization is the transfer of a hydride from the coordinating benzene to C1. In the catalytic cycle suggested by Periana et al.,[5] two possible mechanisms for the hydride transfer were presented, one stepwise mechanism featuring a seven coordinate Ir^V intermediate and one concerted σ-bond metathesis type mechanism. We were not able to locate any stable intermediates, as all starting geometries eventually converged to **16** or **17**. However, a transition state **TS3** connecting **16** and **17** was easily located. **16** → **TS3** has an

Table 2. Relative Energies and Geometry Parameters for Regio-Isomers of **TS2**

		experimental data[a]			relative energies (kcal/mol)				bond lengths (Å)			
olefin	isomer	TOF	ratio	$\Delta\Delta G^b$	ΔH(0 K)	$\Delta\Delta H$(0 K)	ΔG	$\Delta\Delta G^b$	Ir–C1	C1–C2	C2–C3	Ir–C3
ethene	N/A	420	100	N/A	27.0	N/A	29.3	N/A	2.07	1.47	1.90	2.20
propene	1,2	110	61	0.4	29.8	0.4	33.7	0.6	2.08	1.47	1.88	2.20
	2,2		39		30.2		34.3		2.07	1.47	1.94	2.20
iso-butene	1,2	3	82	1.4	34.1	0.7	37.9	1.2	2.09	1.49	1.85	2.21
	2,2		18		34.8		39.1		2.06	1.48	1.98	2.21
styrene	1,2	180	98	3.5	31.8	2.4	36.7	2.5	2.11	1.47	1.88	2.20
	2,2		2		34.1		39.2		2.07	1.47	1.97	2.21
VTFM	1,2				24.8	6.1	29.1	7.9	2.08	1.47	1.93	2.19
	2,2				30.9		37.0		2.08	1.46	1.97	2.18
VME	1,2				30.0	−4.0	34.5	−2.5	2.08	1.46	1.90	2.19
	2,2				26.0		32.5		2.07	1.47	1.98	2.19

[a] From ref 3. [b] Recalculated for 298 K.

energy barrier of 12.0 kcal/mol and a negative eigenvalue of -391 cm^{-1} corresponding to movement of the hydride. However, **TS3** does *not* correspond to a σ-bond metathesis transition state.

The structure for **TS3** in Figure 8 shows that the Ir−H distance is only 1.58 Å, which is a normal Ir−H sigma bond. However, the H−C bond being broken on the benzene has increased from 1.09 Å to 1.99 Å, whereas the benzene C−Ir bond has decreased from 2.39 Å to 2.09 Å, essentially a full Ir−C sigma bond. At the same time, the new C−H bond is 1.69 Å while the Ir−C1 bond being broken has increased from 2.10 Å to 2.21 Å. The C···H···C angle is 154°. **TS3** is consequently best described as Ir^{V} with three covalent bonds to phenyl, H, and C1 in addition to the two to acac†'s. The H has essentially no bond to either C1 or to the phenyl. *Clearly this is not σ-bond metathesis.* This process of **16** → **TS3** → **17**, we refer to as "*oxidative hydrogen migration*". This is the first documented example of this type of transition state, which will be further discussed in section 3.6.

The product of **TS3** is the intermediate **16**, which now features a covalently bound phenyl and an ethyl benzene loosely coordinated through an H−Ir Lewis acid-Lewis base (LA−LB) interaction. The net energy change from **16** to **17** is 0.1 kcal/mol downhill.

3.4.5 Product Formation (17 → 11 + 3). Dissociation of the ethyl benzene from **17** to yield the product **3** is uphill by 2.9 kcal/mol, but barrierless. This involves breaking the CH−Ir LA−LB bond, which is partially compensated by the energy gained through Ir−Ph back-bonding.

3.4.6 Regeneration of the Catalyst (11 + ethylene → 9). Coordination of a C_2H_4 molecule to the vacant site of **11** is exothermic by 26.6 kcal/mol (and barrierless), leading back to **9** and completing the catalytic cycle. The final energy for **9** + **3** in Figure 7 is 21.7 kcal/mol lower than the **9** in Figure 6, corresponding to the calculated exothermicity of the reaction.

We find that the rate-determining step for the catalytic cycle is going through **TS2**, the migratory insertion. For catalyst **7** we calculated this activation energy to be 27.0 kcal/mol. We also calculated **TS2** for the **4** catalyst, where we obtain 25.2 kcal/mol, corresponding to the ground-state effect discussed in section 3.2.

The experimentally determined activation energy for **4** is 28.7 kcal/mol,[3] in excellent agreement with the calculated value of 25.2 kcal/mol.

3.5 Regioselectivity of Olefin Insertion. On the basis of our calculated mechanism, the origin of the regioselectivity rests in the energies of the various conformers in **TS2**. To confirm this, we carried out calculations of **TS2** with several substituted olefins and compared the relative energy barriers with the experimentally measured ratios. Pertinent geometry values and relative energies are given in Table 2.

The simplest substituted olefin investigated by Periana and Matsumoto is propene, which gives linear and branched propyl benzene in a 61:39 ratio, which at 180 °C (453 K) corresponds to a $\Delta\Delta G$ of 0.4 kcal/mol in favor of the linear product. Our calculations of **TS2**-propene show that the lowest energy isomer of **TS2**-propene, labeled **TS2**(1,2)-propene, has a relative energy of 29.8 kcal/mol and is expected to yield linear propyl benzene. The lowest energy isomer that leads to a branched propyl benzene is **TS2**(2,2)-propene, with a relative energy of 30.2 kcal/mol. Other isomers of **TS2** were optimized, but were found to be over 1 kcal/mol higher in energy and will not be further discussed. Our calculated $\Delta\Delta H$ (0 K) value is thus 0.4 kcal/mol, remarkably close to the experimental $\Delta\Delta$G value. Inclusion of calculated ΔG terms lead to a $\Delta\Delta G$(453 K) value of 0.6 kcal/mol, also very close to the experimental value.

Calculations of **TS2**(1,2)-isobutene and **TS2**(2,2)-isobutene gave structures with relative energies of 34.1 and 34.8 kcal/mol, respectively, and a $\Delta\Delta H$(0 K) of 0.7 kcal/mol, which should be compared to the experimental value of 1.4 kcal/mol. Inclusion of ΔG terms yields a $\Delta\Delta G$(453 K) of 1.2 kcal/mol. Both $\Delta\Delta H$ and $\Delta\Delta G$ are very close to the experimental value.

Our investigation of **TS2**-styrene was limited to the isomers **TS2**(2,2)-styrene and **TS2**(1,2)-styrene, with the expectation that these are the lower energy structures of each pathway. The relative energy of **TS2**(1,2)-styrene and **TS2**(2,2)-styrene are calculated to 31.8 and 34.1 kcal/mol, respectively, which gives a $\Delta\Delta H$(0 K) value of 2.3 kcal/mol. Inclusion of ΔG terms yields a $\Delta\Delta G$(453 K) of 2.5 kcal/mol. With an experimental $\Delta\Delta G$(453 K) value of 3.5 kcal/mol, both $\Delta\Delta H$ and $\Delta\Delta G$ are ∼1 kcal/mol from the experimental value. This error could be due to a well known problem in DFT for the correct treatment of Van der Waals interactions, particularly for pi-stacking systems like **TS2**(2,2)styrene. However, it could also be experimental error in the original publication. The ratio of 1,2-diphenylethane:1,1-diphenylethane is reported as 98:2, which corresponds to a $\Delta\Delta G$(453 K) of 3.5 kcal/mol. The value 2.4 kcal/mol corresponds to a ration of 95:5, possibly within the margin of error. Nevertheless, it is clear that our calculations reproduce both the trend and the magnitude of experimental $\Delta\Delta G$ values.

We also considered the underlying causes of the regioselectivity. One factor is the steric bulk of the olefin substituents.

The bond lengths in Table 2 show that the calculated Ir−C3 and C1−C2 distances are essentially identical for all four olefins investigated here, independent of regio-isomer. On the other hand, the Ir−C1 and C2−C3 distances are affected just as would be expected for steric crowding, i.e., increasing when the carbon center is substituted. Furthermore, using **TS2**-ethene as a base point, we see that substitution at C1 results in deviations ≤0.04 Å, whereas substitution at C2 yields C−Ph changes of ≤0.07 Å. Consequently, we expect substitutions at C1 to be advantageous. Inspection of the optimized geometry of **TS2**(1,2)-propene suggests that the substituent fits into the empty space above the acac† unit, whereas the substituent in **TS2**(2,2)-propene is crowded against the phenyl group.

However, sterics alone do not account for the substantially higher linear/branched ratio of styrene vs. isobutene. Phenyl is less bulky than methyl, and insertion in styrene should thus be less selective. Consequently, there must be an electronic factor, which we believe is an electron-donating/withdrawing character. Iridium is more electron rich than carbon, and it would thus be more advantageous for an olefin with an electron withdrawing substituent to form **TS2**(1,2) over **TS**(2,2). This is consistent with the substituents explored above, as the linear/branched ratio increases in the order propene < isobutene < styrene.

Neither methyl or phenyl are particularly electron withdrawing, however; so to explore our hypothesis, we sought more electronically active substituents. The only available substituent in ref 5 is methyl ethyl-phenyl ester, which has an experimental linear:branched ratio of 69:31. However, although the ester group is electron withdrawing, it is also significantly less bulky than methyl or phenyl, which most likely causes the low selectivity. With a $\Delta\Delta G$ value of merely 0.7 kcal/mol this substituent is not a suitable target for testing of our hypothesis.

Instead, we optimized the regio-isomers of vinyl trifluoromethyl, VTFM, and vinyl methyl ether (VME). VTFM is a very electron poor olefin and should consequently give a high percentage of linear products, whereas VME is an electron rich olefin which should give high percentage of branched products. Our results, summarized in Table 2, show that **TS2**(2,2)-VTFM and **TS2**(1,2)-VTFM have calculated relative energies of 30.9 and 24.8 kcal/mol, respectively, which gives a $\Delta\Delta H$(0 K) of 6.1 kcal/mol. **TS2**(2,2)-VME and **TS2**(1,2)-VME have calculated relative energies of 26.0 and 30.0, respectively, which gives a $\Delta\Delta H$(0 K) of −4.0 kcal/mol. This suggests that electron donating character is much more important than steric bulk, to the point of reversing regio-selectivity for a particularly electron donating substituent. These theoretical predictions are currently awaiting experimental verification.

The electronic trend calculated above closely mirrors the trend observed in the Heck reaction. This is not surprising, since both reactions undergo a 1,2-insertion with similar geometries (see Figure 12).[22] This is promising for the development of a more active catalyst, as we can draw on the large body of both mechanistic and empirical knowledge gathered for Heck type chemistry. Steric effects appear to be more important than in the Heck insertion, however, most likely due to a shorter distance in the forming C2−C3 bond. The C2−C3 distances in **TS2**(2,2)-propene and **TS2**(1,2)-propene, for example, are 1.94 Å and 1.88 Å, respectively, whereas the C2−C3 distances in the Heck insertion transition structures are 2.17 Å and 2.13 Å, respectively.[22b] The metal−C1 distances, on the other hand, remain between 2.08 Å and 2.13 Å for both **TS2** and the Heck insertion.

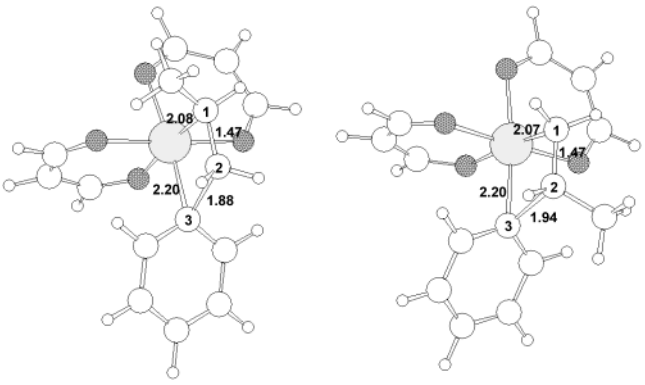

Figure 11. **TS2**(1,2)-propene and **TS2**(2,2)-propene. Distances in Angstroms (Å).

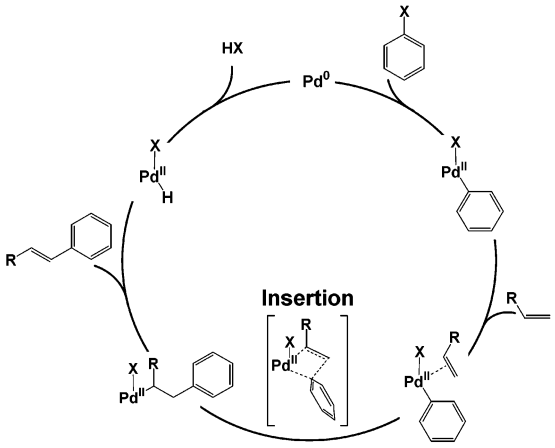

Figure 12. Heck reaction.

3.6 C−H Activation. What makes this catalyst unique is that unlike the Heck reaction, it also features C−H activation. As such, the activation mechanism deserves further consideration, even though it is not the rate determining step. In the catalytic cycle suggested by Periana et al.[5] two possible mechanisms for the C−H activation were presented, one stepwise mechanism featuring a seven coordinate Ir^V intermediate and one concerted σ-bond metathesis type mechanism. On the basis of precedents from the groups of Bergman[6] and Maitlin,[7] we expected the stepwise mechanism to be the lower energy pathway. However, our calculations do not lead to seven coordinate Ir^v intermediates. Depending on starting structure, all starting geometries converged to either **15** or **16**.

To ensure that this result is not an artifact of the computational methods employed in this study, we optimized the seven coordinate Ir^V intermediate $[Cp^*(PH_3)Ir(CH_3)_2(H)]^+$ from ref 6, and found that our geometries corresponded very closely to the Ir^V geometries characterized by the groups of Chu[23] and Hall.[24]

We suggest that there are two major differences between the Bergman and Periana compounds responsible for this very different behavior.

(22) Ludwig, M.; Stromberg, S.; Svensson, M.; Akermark, B. *Organometallics* **1999**, *18*, 970. (b) Schenk, H.; Stromberg, S.; Zetterberg, K.; Ludwig, M.; Akermark, B.; Svensson, M. *Organometallics*, **2001**, *20*, 2813.

(23) Su, M.-D.; Chu, S.-Y. *J. Am. Chem. Soc.* **1997**, *119*, 5373.
(24) Niu, S.; Hall, M. B. *J. Am. Chem. Soc.* **1998**, *120*, 6169.

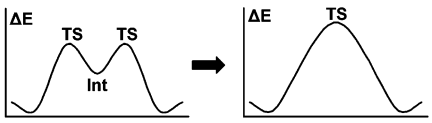

Figure 13. C−H activation energy profile changes with reduced Ir electron density.

First: the presence of the η-5 aromatic Cp* ligand in the Bergman compound is less bulky than the three separate ligands in the Periana compound. All published examples of seven coordinate $L_4Ir^V(R)(H)(R)$ species have either Cp* or cyclooctadiene present as L_3 or L_2, respectively.

Second: the electron densities on the iridium atoms are quite different. The ligands in the Bergman compound $[Cp^*(PH_3)Ir(CH_3)]^+$ are electron donating,[6] resulting in a calculated Mulliken charge of −0.29 electrons on the iridium. In contrast the Mulliken charge on the iridium in **11** {the structure corresponding most closely to $[Cp^*(PH_3)Ir(CH_3)]^+$} is 0.76 electrons, a difference of over one electron. Clearly, oxidizing Ir^{III} to Ir^V is less favorable for a structure with a much higher positive charge on the metal center.

It is interesting that Chu and Hall concluded that there is no concerted transition structure on the $[Cp^*(PH_3)Ir(CH_3) + CH_4]^+$ hyper surface, which is in stark contrast to our finding of the asymmetric transition structure **TS3**. We suspect that **TS3** has much more in common with the intermediate $[Cp^*(PH_3)Ir(CH_3)_2(H)]^+$ than any of the transition states in the Chu and Hall studies. With an electron rich Ir^{III} center, the mechanism for C−H activation is stepwise and low in energy, while reducing electron density gradually increases the relative energy of the intermediate until the mechanism obtains concerted character, as illustrated in Figure 13.

3.7 β-Hydride Elimination as an Alternative Mechanism. β-Hydride elimination is normally quite facile for late transition metals,[25] and there is no reason to believe Ir to be an exception. Indeed, it is the major reactive pathway for (PCP)Ir catalyzed dehydrogenation of ethane as reported by Goldman and coworkers.[26] β-hydride elimination leading to styrene is also thermodynamically feasible (eq 2) in the ethylene/benzene system if a second ethylene is used as a sacrificial hydrogen acceptor.[18] Nevertheless, as seen in the publications of Matsumoto[2−4] and Periana,[5] no styrene byproducts were observed from arylation of olefins with catalysts **4**−**8**. However, Matsumoto et al. reported that adding $O_2/Cu(OAc)_2$ (a potential hydride scavenging oxidizing agent) to catalyst **1** in a mixture of benzene and ethene generated exclusively styrene and vinyl acetate, but with significantly lowered yield.[27]

$$C_2H_4 + C_6H_6 \rightarrow \text{styrene} + C_2H_6 \quad \Delta H^\circ = -29.7 \text{ kcal/mol} \tag{2}$$

It is thus relevant for us to consider β-hydride processes to understand these experiments and to ensure that we have considered all plausible reactions. We investigated the production of styrene from benzene and ethene with the results summarized in Figure 14, where we have indicated with dotted lines the catalytic cycle for reference purposes. The structures of **TS4** and **18** are shown in Figure 10.

As **15** is the only coordinately unsaturated intermediate in the catalytic cycle, we assumed that β-hydride elimination would occur from this part of the hypersurface. However, the energy of the optimized transition structure for this elimination, **TS4**, is 7.6 kcal/mol lower than **15**, indicating that **15** need not play a role in β-hydride elimination.

The only prerequisite for **TS4** is an Ir−C−C−H dihedral of ∼0°, and this can be achieved through a rotation around the Ir−C−C−Ph dihedral in **14** by ∼81°. The actual Ir−C−C−H dihedral in **TS4** is 5.6°, reflecting a small steric interaction between the phenyl group and one of the acac†-rings. **TS4** is an early transition structure, with almost unchanged Ir−C and C−C distances of 2.07 Å and 1.48 Å, respectively. The breaking C−H bond is increased to 1.36 Å and the forming Ir−H bond is decreased to 1.70 Å.

Completing the process yields structure **18** with an energy of 9.5 kcal/mol below **14**. In **18** the styrene is strongly coordinated with short Ir−C distances of 2.16 and 2.25 Å, (much like the ethene in **9** with 2.21 Å). Thus, dissociating styrene from **18** to form **19** + **20** is 28.5 kcal/mol uphill, about the same as the bond of 26.6 of ethene to **11**.

Because the maximum barrier from **14** through **TS3** to ethyl benzene product in Figure 7 is 11.0 compared to 19.0 kcal/mol for the barrier to form styrene, we consider that styrene should not been formed under the conditions we consider here. It should be pointed out that this is contrary to the conclusions drawn from the ΔG surface, where styrene formation through **19** + **20** is favored by 3.3 kcal/mol compared to **TS3**. However, as discussed in sections 2 and 3.9, the accuracy of the ΔG surface deteriorates rapidly when the number of species changes in the solution, and we believe that the ΔH surface is considerably more reliable.

However, we also calculated potential products of **19**. Isomerization of the cis hydride **19** to the trans hydride **23** goes through **TS5** with a barrier of 2.6 kcal/mol. This cis to trans reaction is exothermic by 20.7 kcal/mol, which can be compared to 19.6 kcal/mol for the phenyl case (**11** versus **10**). Finally, coordination of an ethene to **23** gives structure **24**, which is downhill by 3.9 kcal/mol.

Instead of isomerizing to the trans-acac† geometry, **19** could coordinate directly with an ethene, leading to structure **21** which is exothermic by 32.9 kcal/mol. **21** could form an $Ir-CH_2CH_3$ structure, **22**, via ethene insertion in the Ir−H bond. This is endothermic by 3.9 kcal/mol and may have an additional barrier.

22 could in turn react with a benzene via a transition structure similar to **TS3**. The product of this reaction chain could potentially regenerate the catalyst into **9**, with the use of a sacrificial ethene to yield ethane.

This reaction pathway is calculated to be exothermic by 27.0 kcal/mol, which is 5.3 kcal/mol more exothermic than the production of ethyl benzene. That this thermodynamically favored product is not observed is consistent with our result that the barrier from **18** to **21** is much higher than that from **14** through **TS3**.

However, a hydride scavenging agent such as $Cu(OAc)_2$ would likely react with a hydride intermediate such as **18** to generate a five coordinate Ir^{III} cation, which could react further to regenerate the catalyst. This would bypass the high-energy

(25) Zaera, F. *Appl. Catal. A: General* **2002**, *229*, 75.
(26) Liu F. C.; Goldman, A. S. *Chem. Commun.* **1999**, 655−656. (b) Liu F. C.; Pak E. B.; Singh B.; Jensen C. M.; Goldman A. S. *J. Am. Chem. Soc.* **1999**, *121*, 4086. (c) For a theoretical study, see Li, S. H.; Hall M. B. *Organometallics* **2001**, *20*, 2153.
(27) Matsumoto, T.; Periana, R. A.; Taube, D. J.; Yoshida, H. *J. Cat.* **2002**, *206*, 272.

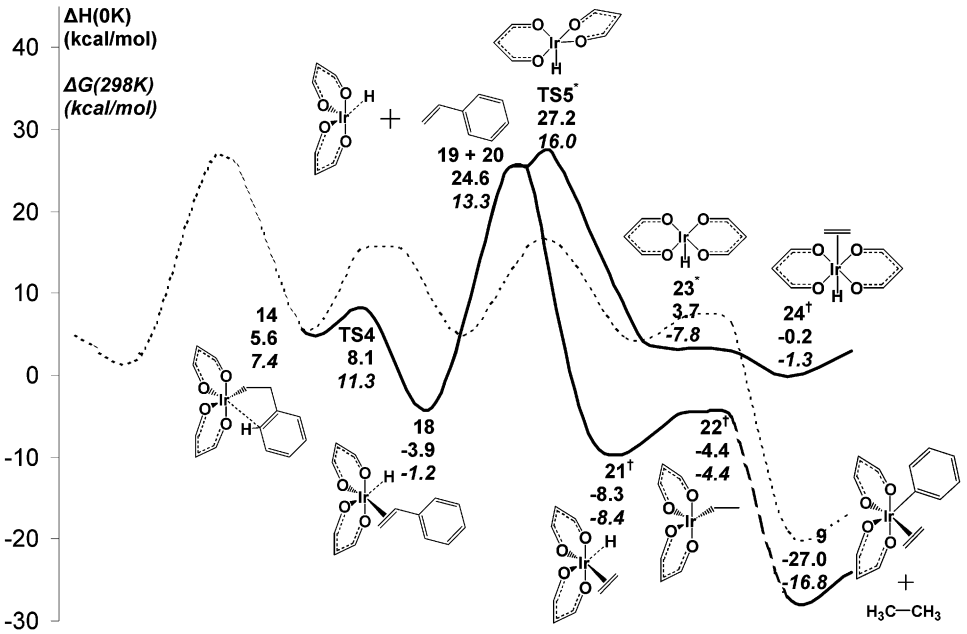

Figure 14. Mechanism for β-hydride elimination of **14** to form styrene. *Energies include loss of styrene †Energies include loss of styrene and addition of ethene.

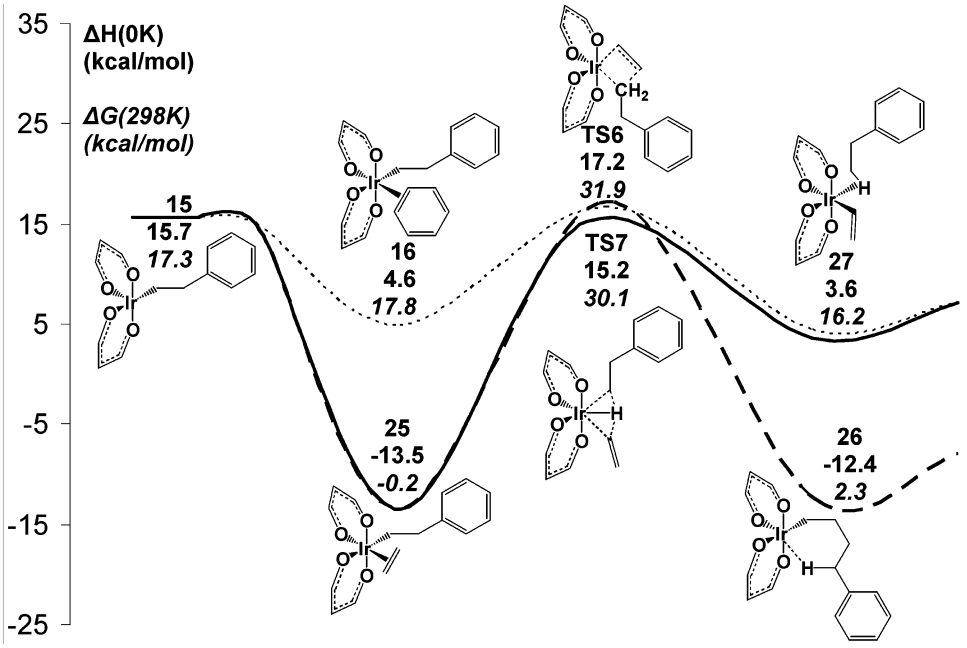

Figure 15. Inhibition by ethylene. Mechanistic pathway from section 3.4 included in dotted line. Insertion pathway from **25** in dashed line, hydrogen migration pathway from **25** in solid.

pathway through **19**, resulting in exclusive formation of styrene and byproducts. More detailed theoretical and experimental investigations of the $Cu(OAc)_2$ and related systems are warranted and planned for future studies. We are also currently trying to confirming the rapid equilibrium between **15** and **18** by labeling studies.

3.8 Inhibition by Ethene. Although the TOF is reported to rise with increased ethene/benzene molar ratio at low ratios, it drops again above a ratio of ~0.20.[3] As our calculations of intermediates **9** and **12** shows, a ground state effect is not the cause of the inhibition, which leaves inhibition of a key mechanistic step as the cause of the inhibition. The only likely candidate for this step is the five coordinate intermediate **15**. Our calculations show that coordination of an ethene to **15** gives structure **25**, (see Figure 15) which is exothermic by 29.2 kcal/mol (similar to the 26.6 kcal/mol for **11** to **9**). This is significantly more favorable than the next intermediate on the catalytic cycle, **16**. However, since the coordination of either ethene or benzene to **15** is barrierless, we estimate that the relative rate of formation of **16** vs **25** should be proportional to the ratio of ethene to benzene concentrations in a purely statistical fashion.

From **25**, we considered three mechanisms. The first is simply reversal of the previous step, i.e., dissociation of the ethene molecule to regenerate structure **15**, which would then be followed by association of either ethene or benzene. Although

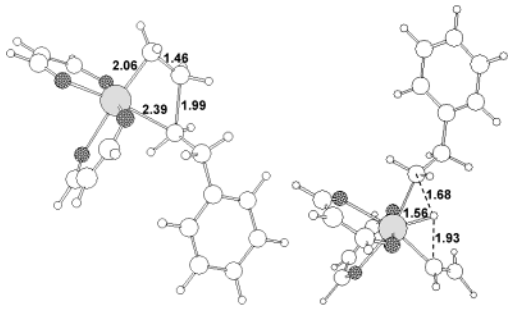

Figure 16. **TS6** and **TS7**. Distances in Angstroms (Å).

the dissociation is barrierless, we can consider the difference in energy between **25** and **15** as the activation energy of this process, which would then be 29.2 kcal/mol.

The second possibility is a reaction analogous to **9** → **TS2** → **14**, where the $-CH_2-$ group is inserted into the π bond via the transition structure **TS6**, 30.7 kcal/mol higher in energy than **25**. The slightly higher activation energy (24.5 kcal/mol for **9** → **TS2**, compared to 30.7 for **25** → **TS6**) reflects the somewhat lower migratory aptitude of a $-CH_2-$ vs a -phenyl moiety. This can also be seen in the geometry of **TS6** (see Figure 16), where the relevant bond distances are Ir−C1′ = 2.06 Å, C1′−C2′ = 1.46 Å, C2′−C3′ = 1.99 Å and C3′−Ir = 2.39 Å, which should be compared to the bond distances in **TS2**: 2.07, 1.47, 1.90, and 2.20 Å, respectively. It is clear that C3′ in **TS6** is significantly further away from both Ir and C2′ than C3 in **TS2** is from Ir and C2. **TS6** leads to the longer chain phenyl alkane complex **26**, which could potentially undergo further reaction either with benzene or ethene.

The third possible reaction is a hydrogen migration analogous to **16** → **TS3** → **17**, where one of the hydrogens from the ethene migrates to the $-CH_2-$ moiety via **TS7**, 28.7 kcal/mol higher in energy than 25. This transition structure is very similar to **TS3**, with a Ir−H distance of 1.56 Å and C−H distances of 1.93 Å and 1.67 Å (see Figure 16). The significantly higher activation energy of **25** → **TS7** (28.7 kcal/mol) than **16** → **TS3** (12.0 kcal/mol) is caused by ground-state stabilization.

Comparing the activation energies of the dissociation (29.2 kcal/mol), insertion (30.7 kcal/mol) and hydrogen migration (28.7 kcal/mol), we conclude that hydrogen migration is the most favorable. However, we must note that the difference in calculated activation energies is at most 2.0 kcal/mol, which is within the margin of error for these types of calculations. Nevertheless, it is encouraging to see that our calculations show a higher energy for **TS6** than either **TS7** or **15**, as this is consistent with the lack of polymerization products. Furthermore, the preference of hydrogen migration over dissociation is of little practical significance, as both mechanisms eventually yield structures **3** and **9**. The complete mechanism of the subsequent steps has also been calculated and will be discussed in a future publication.

It is clear that regardless of mechanism, the association of ethene causes inhibition. The lowest calculated activation energy for reaction of **25**, 28.7 kcal/mol, is higher than the activation energy of the rate-determining step in the catalytic cycle, **TS2**, at 27.0 kcal/mol. As such, the association of ethene introduces a new rate determining step in the reaction which is consistent with the experimental observation. We are currently trying to isolate or independently synthesize intermediate **25** for further experimental verification.

Because the energy of **TS3** is similar to **15**, we expect about half the **16** formed will proceed through **TS3** to form ethyl benzene product, whereas the other half might revert back to **15**, making it vulnerable again to ethene inhibition. If the energy of **TS3** were significantly higher than **15**, this reasoning would suggest that the catalyst might become inactive, even though **TS3** is lower in energy than **TS2**. Consequently, for the reaction to proceed at a reasonable rate in the presence of significant amounts of ethylene, the catalyst should have a **TS3** with equal or lower relative energy than **15**. This naturally poses additional difficulties in designing catalyst with improved activity than the ones previously characterized.

3.9 Discussion of Accuracy. 3.9.1 ΔG Calculations. The ΔH and ΔG values are fairly similar for reactions having the same number of reacting molecular fragments, as the translational and rotational components are similar. Thus, the process **7** + C_2H_4 → **9** + H_2O has a calculated ΔH(0 K) of 2.5 kcal/mol, and a calculated ΔG(298 K) of 4.5 kcal/mol. This total ΔG correction of 2.0 kcal/mol most likely reflects a lower rotational barrier for the H_2O group. In addition, the relative energy change from **7** to **TS2** is ΔH = 27.0 and ΔG = 29.3 kcal/mol, which is consistent with the experimentally determined activation energy of 28.7 kcal/mol.

However, for a process such as association of benzene to **15** to form **16** there are much larger corrections. For **15** + C_6H_6 → **16** is ΔH(0 K) = −11.1 kcal/mol, whereas ΔG(298 K) = +0.5 kcal/mol. Similarly **16** → **TS3** has activation energies of ΔH = 15.6 and ΔG = 30.7 kcal/mol, because **TS3** is very constrained. As a result the ΔG for **TS3** is 1.4 kcal/mol higher in energy than **TS2**, whereas ΔH is 10.4 kcal/mol lower.

However, we should point out that the entropies have been calculated for the gas-phase system. We have not tried to include the vibration energies of the molecules in solvation, nor the diffusional motions, both of which will decrease the free entropy for the free reagents, making the results closer to the ΔH numbers.

3.9.2 Concentration Effects. We have made no attempt to correcting our free energies for concentration effects. For example, the **15** + C_6H_6 → **16** has a calculated ΔG = 0.5 kcal/mol. Correcting for the concentrations according to eq 3, reduces the free energy by RT_ln($[C_6H_6]^{-1}$), which in neat benzene is equal to 1.4 kcal/mol.

$$\Delta G = \Delta G^\circ - RT\cdot\ln([\mathbf{16}]\cdot[\mathbf{15}]^{-1}\cdot[C_6H_6]^{-1}) \qquad (3)$$

3.9.3 Solvation Corrections. For a molecule in a solvent, there will be entropy corrections from the vibrational states. This is not included in the continuum solvent approximation. These corrections could be included using molecular dynamics with explicit solvents, which unfortunately is beyond the scope of this study.

3.10 Rational Improvement of Catalyst Activity. The ultimate goal of this mechanistic study is to improve the catalyst. On the basis of our understanding of the mechanism of 1,2-insertions, we expect that a catalyst with less electron density on the metal would have a lower activation energy. To confirm this assumption, we optimized two analogues to **7** and **TS2**-ethene, where the acac† groups were modified with electron donating and electron withdrawing groups. The results of these studies are summarized in Figure 17.

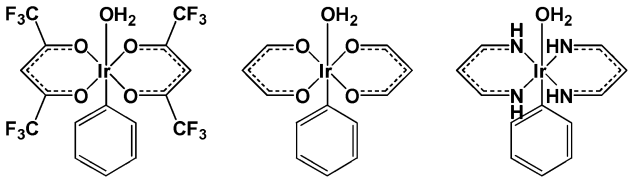

Figure 17. Structures **4CF3**, **7** and **4N**.

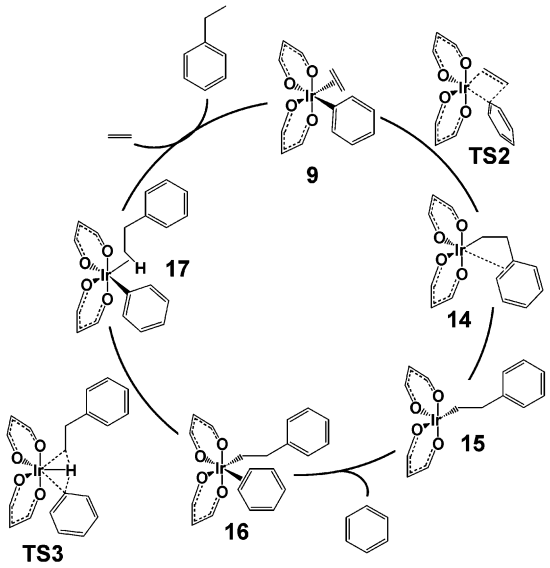

Figure 18. Catalytic Cycle.

3.10.1 Electron Donating Substituents. In compound 4N, the carbonyls of the two acac†s are replaced with imines, which are more electron donating. We find that this increases the $\Delta H(0\ \mathrm{K})^{\ddagger}$ for **7** to **TS2** from 27.0 to 34.8 kcal/mol. Thus, electron donating substituents should substantially decrease the rate.

3.10.1 Electron Withdrawing Substituents. In the second system, labeled **4CF$_3$**, the four hydrogen groups of the acac† were replaced with electron withdrawing $-CF_3$ groups. We find that this reduces the $\Delta H(0\ \mathrm{K})^{\ddagger}$ for **TS2** from 27.0 to 23.0 kcal/mol, which should substantially improve the rates. Control calculations on **TS3** showed only marginal change, with $\Delta H(0\ \mathrm{K})^{\ddagger}$ going from 16.6 to 15.9 kcal/mol.

4. Summary and Conclusions

We find that (L)Ir(acac†)$_2$ catalyzed arylation of olefins reacts through a mechanism with two key steps, 1,2-insertion and oxidative hydrogen migration.

The insertion is rate determining, with a calculated $\Delta H(0\ \mathrm{K})^{\ddagger}$ of 25.2 kcal/mol for the dimeric catalyst **4**. The activation energy increases with increased electron density on the coordinating olefin, as well as increased electron donating character on the ligand system. The regioselectivity is shown to depend on the electronic and steric character of the olefin, where steric bulk and electron withdrawing character favors linear product formation.

Activation of the C−H bond occurs through a novel concerted oxidative hydrogen transfer mechanism in which a hydrogen migrates from a coordinating benzene to the covalently bound phenyl alkyl through a transition structure in which the H is bonded to the metal and not either carbon. The metal transforms from Ir^{III} to Ir^{V} in establishing this unusual transition state.

Activation of the precatalyst occurs through a dissociative pathway, where the ligand L first dissociates, followed by a rearrangement of the trans-acac†groups into a cis conformation, which is stabilized by association of an ethylene. The calculated $\Delta H(0\ \mathrm{K})^{\ddagger}$ is 35.1 kcal/mol and $\Delta G(298\ \mathrm{K})^{\ddagger}$ is 26.1 kcal/mol. The nature of L influences the speed of the reaction through a ground-state effect—a high energy Ir−L coordination lowers the relative energy of the starting catalyst, but does not affect the relative energy of the rate determining step.

We investigated the possibility of a β-Hydride elimination mechanism. We find that it is facile but reversible, with all further reactions kinetically unfavorable.

We also considered inhibition by excess olefin which we find is caused by competition between olefin and aryl for an intermediate in the catalytic cycle.

Although we calculated the ΔG values for the various processes, we are not confident that the entropy in solvation is adequately treated. In addition, we have not corrected for concentration effects.

On the basis of the mechanism, we suggest that including electron withdrawing substituents on the acac ligands, such as trifluoromethyl groups, would increase the activity.

Acknowledgment. We gratefully acknowledge financial support of this research by the ChevronTexaco Energy Research and Technology Co., and thank Dr. William Schinski of ChevronTexaco for helpful discussions. We also wish to thank Guarav Bhalla and Dr. Xiang Yang Liu for suggestions and insights.

Supporting Information Available: Tables of geometries, imaginary frequencies, and absolute energies. This material is available free of charge via the Internet at http://pubs.acs.org.

JA034126I